BLACK HOLE SPACETIMES: TESTING NUMERICAL RELATIVITY

David H. Bernstein, David W. Hobill, and Larry L. Smarr
National Center for Supercomputing Applications
605, East Springfield Avenue
Champaign, IL 61820

Abstract. Spherically symmetric black hole spacetimes are studied numerically using the standard 3+1 decomposition of the Einstein equations. Different finite difference methods are employed and the results are compared with the known analytic behavior of the Schwarzschild solution. A discussion of coordinate and gauge conditions is included and it is demonstrated that, given the appropriate combinations of finite difference methods and gauge choices, free evolution can accurately propagate the constraint equations.

I. INTRODUCTION

The numerical construction of black hole spacetimes provides an opportunity to study the purely geometrodynamical effects of the gravitational field. Along with vacuum cosmologies and pure gravitational radiation, these spacetimes yield important information concerning the nonlinear behavior of gravitational fields that have been freed from the influences of matter or other fields. One of the advantages of studying black hole spacetimes is that analytic initial data sets exist describing various configurations for N black holes (see the article by York in this volume). The solutions are obtained by modelling the black holes with Einstein-Rosen bridges connecting two isometric sheets. The boundary separating the two sheets (known as the throat) provides unambiguous inner boundary conditions for the construction of numerical solutions. Further simplifications arise if the initial data is assumed to be time symmetric.

Since one of the major goals of this project is to re-calculate the original Smarr-Eppley (1979) axisymmetric two black hole collision using modern numerical methods and the power of a supercomputer, we have begun with the careful construction of a code that is able to reproduce a number of well known analytic results concerning the behavior of black hole spacetimes. The most obvious verification of any black hole code would be that it reproduce the Schwarzschild spacetime. In the two black hole collision, for example, this spherically symmetric spacetime can be thought of as the solution at late times when all of the radiation has propagated away, or the solution in the limit that the mass of one of the black hole vanishes. Therefore, reproducing the Schwarzschild solution using the methods that will be employed for the two-black hole collision is of fundamental significance and will act as an important test-bed calculation.

In the next section different choices of gauges and coordinates useful for numerically constructing spherically symmetric spacetimes will be presented. In Section III we will discuss the different finite difference techniques that are employed, and the fourth section

presents a brief review of the analytic behavior associated with the Schwarzschild solution and its relevance to the numerical results. Finally we discuss the propagation of the constraints by the finite differenced version of the Einstein equations and include a discussion of the next phase of this project and the tests that will have to be met before continuing on to the two black hole collision.

II. COORDINATE AND GAUGE CHOICES FOR BLACK HOLE SPACETIMES

In constructing analytic solutions of the Einstein equations whether they be in exact, closed form or the result of a perturbative scheme, one frequently chooses coordinates and gauges that simplify certain aspects of the field equations. The same point holds true for the construction of numerical solutions of the Einstein equations. Different gauge choices can be made either to simplify the equations or relate them more intimately to the geometry of the spacetime. We begin with the standard 3+1 (or 1+1 for spherical symmetry) decomposition of the Einstein equations.

The most general line element for spherical symmetry is

$$ds^2 = (-\alpha^2 + A\beta^2)\,dt^2 + 2A\beta\,dt\,dr + A\,dr^2 + Br^2\,d\theta^2 + Br^2\sin^2\theta\,d\phi^2 \qquad (2.1)$$

where where α is the lapse function, $\beta=\beta^r$ is the shift vector (one component with spherical symmetry), and $\gamma_{ij} = \mathrm{diag}(A, Br^2, Br^2\sin^2\theta)$ is the 3-metric on a t=const. hypersurface. All the metric coefficients are functions of t and r. For the construction of numerical solutions of the Einstein equations, many authors have followed the suggestion of Wilson (1979) that a simplification of the evolution equations can be brought about through *algebraic* coordinate conditions on the 3-metric. Historically two choices have dominated research in both spherical and axial symmetry. Radial gauge used by Estabrook et. al.(1973), Bardeen & Piran (1983) and Choptuik (1983) sets B=1. The well known Schwarzschild coordinates are a prime example of this gauge choice where:

$$\alpha=(1-\frac{2m}{r})^{1/2} \qquad A=(1-\frac{2m}{r})^{-1} \qquad B=1 \qquad (2.2)$$

The other coordinate system, the quasi-isotropic or isothermal gauge, has been used by Evans (1986), Shapiro & Teukolsky (1986) and Choptuik (1983) and is distinguished by setting A=B. The Schwarzschild solution is also well known in these coordinates:

$$\alpha=\frac{(1-\frac{m}{2r'})}{(1+\frac{m}{2r'})} \qquad A=B=(1+\frac{m}{2r'})^4 \qquad (2.3)$$

where $r=(1+m/2r')^2r'$ relates the Schwarzschild and isotropic coordinates. In eqs. (2.2) and (2.3) the solution is explicitly time independent and the shift vanishes.

In the 3+1 decomposition of a spacetime, the extrinsic curvature of the spatial hypersurfaces

$$K_{ij}=(D_i\beta_j+D_j\beta_i-\partial_t\gamma_{ij})/2\alpha \qquad (2.4)$$

expresses how these 3-surfaces are embedded in the four dimensional spacetime. Here D_i is the covariant derivative on the 3-surface. Substituting the conditions placed upon the 3-metric by the radial and isothermal gauge choices into eq. (2.4), one obtains the following conditions on the shift: in radial coordinates $\beta=\alpha K^\theta{}_\theta/r$ while in isothermal coordinates $(\beta/r)_{,r}=\alpha(K^r{}_r-K^\theta{}_\theta)/r$.

In this work, we shall not impose any conditions on the 3-metric, but rather maintain it in its most general form, thereby leaving the choice of the lapse function and shift vector free to explore gauge conditions that are more geometric in nature. This point of view has also been taken by Thornburg (see his contribution to this volume) and is likely to become more popular as the power supercomputers increase. We are now in the position to write out the vacuum Einstein equations in the standard 3+1 form: the constraints may be written as

$$R + (\mathrm{Tr}\ K)^2 + K_{ij}K^{ij} = 0$$
$$D_i(\mathrm{Tr}\ K) - D_k K_i{}^k = 0$$

and the evolution equations are:

$$\partial_t \gamma_{ij} = -2\alpha K_{ij} + D_i\beta_j + D_j\beta_i$$
$$\partial_t K_{ij} = -D_iD_j\alpha + \alpha\,[R_{ij} + (\mathrm{Tr}\ K)K_{ij} - 2K_{ik}K_j{}^k] + \beta^k D_k K_{ij} + K_{kj}D_i\beta^k + K_{ik}D_j\beta^k \qquad (2.5)$$

where R_{ij} and $R = \gamma_{ij}R^{ij}$ are, respectively, the Ricci tensor and the scalar curvature intrinsic to the the 3-space.

Choosing the coordinate system to be in keeping with those used by Cadez (1975) for the two black hole collision problem, we introduce η, a radial coordinate that at t=0 is related to the isotropic radial coordinate by $\eta = \ln(\frac{2}{m}r')$, and $\xi = \theta$. Following the York (1979) prescription for obtaining solutions to the initial vale problem, a conformal factor ψ' (where $A = \psi'^4 a$ and $B = \psi'^4 b$) is factored out of the 3-metric. We then write the line element for the 3-space as $d\sigma^2 = \psi^4 (a\, d\eta^2 + b\, d\Omega^2)$ where $d\Omega^2 = d\xi^2 + \sin^2\xi\, d\phi^2$ and $\psi = \psi' e^{\eta/2}$. The 3+1 form of the field equations in these coordinates along with the expressions for the intrinsic (Ricci) curvature of the spatial hypersurfaces are given in the Appendix. The variables H_a and H_b that appear in the evolution are obtained from the extrinsic curvature written in the conformal form: $K_{ij} = \psi^4 \mathrm{diag}(H_a, H_b, H_b \sin^2\xi)$.

The use of auxiliary variables should be mentioned at this point. The Ricci tensor of the 3-space contains second derivatives of γ_{ij} with respect to η. The field equations as written in the Appendix are in a form that is similar to writing the 1-dimensional wave equation; $\partial_t^2 f - \partial_x^2 f = 0$ as the system: $\partial_t f = h$, $\partial_t h = \partial_x^2 f$ where h is a function that plays the role of the extrinsic curvature. Alternatively the wave equation may also be written in the advective form: $\partial_t g = \partial_x f$, $\partial_t f = \partial_x g$. In this case the temporal and spatial derivatives are both of first order and are treated in the same manner.

For the Einstein equations, the role of the auxiliary variable g could be taken by either the Christoffel symbols [Hahn & Lindquist (1963)] or the first derivative of γ_{ij} with respect to η [Smarr (1979)]. In both of these cases the 3-Ricci tensor can be written in terms of first spatial derivatives and products of the extra variables. As a test of the concept of introducing auxiliary variables, we added the evolution equations for the metric derivatives and the Christoffel symbols to the system (2.5). Unfortunately we found that it was difficult to maintain the stability of the solution beyond 4000 time steps with the Christoffel symbols and 18000 time steps with the metric derivatives (our minimum requirement was 20000 time steps). This result should not be taken as a condemnation of

the use of auxiliary variables since only one test using simple leapfrog finite differencing was made. It is likely that more sophisticated methods will have to be employed in order to make the use of auxiliary variables successful.

Finally, there is the freedom to choose the lapse and the shift. We also choose to provide inner boundary conditions at the throat and this requires that the evolution cover part of the interior of the black hole. This rules out some choices of time slices, e.g. polar slicing which cannot cover the spacetime inside the horizon. We also want to avoid the central singularity by an appropriate gauge choice. The best known of the 'crushing' singularity avoiding time slices is maximal slicing (Tr K= 0) and its properties have been elucidated by Eardley & Smarr (1979). Taking the trace of the extrinsic curvature evolution equation yields:

$$\partial_t(\mathrm{Tr}\ K) = \alpha[(\mathrm{Tr}\ K)^2 + R] - D^i D_i \alpha. \tag{2.6}$$

In the case Tr K=0, eq. (2.6) reduces to an elliptic equation for the lapse that gives the maximal spacelike slices. The problem with a singularity avoiding lapse is that the time slices wrap around the singularity causing large amounts of shear in the coordinate grid. This results in a radial metric coefficient that increases without bound.

The shift vector choices we make explore the differences between Eulerian (normal or β=0) gauge and shifts that minimize the deformations of the geometry from one slice to the other. Smarr and York (1978) describe two such conditions, 1) 'minimal strain', which leads to a linear elliptic equation for β^i:

$$D^i(D_i\beta_k + D_k\beta_i) = D^i(2\alpha K_{ik}) \tag{2.7}$$

and 2) 'minimal distortion' where the distortion tensor is related to the shear of the unit normals to the 3-surfaces.

$$D^i D_i \beta_k + \tfrac{1}{3} D_k(D_i\beta^i) + R_{ik}\beta^i = D^i[2\alpha\,(K_{ik} - \tfrac{1}{3}\gamma_{ik}\mathrm{Tr}\ K)]. \tag{2.8}$$

III. FINITE DIFFERENCING METHODS

This section is concerned primarily with finite differencing methods for the hyperbolic evolution equations. The one elliptic equation that appears in this section comes from eq. (2.6). In the spherical coordinates (η,ξ), the lapse equation yields a two-point boundary value problem for a single second-order ordinary differential equation for α:

$$\partial_{\eta\eta}\alpha + \partial_\eta\alpha\left[\frac{2\partial_\eta\psi}{\psi} + \frac{\partial_\eta b}{b} - \frac{\partial_\eta a}{2a}\right] = \alpha\,(R_{\eta\eta} + \frac{2a}{b}R_{\xi\xi}) \tag{3.1}$$

where $\partial_\eta\alpha = 0$ at the throat and $\alpha = \alpha_{\text{Schwarzschild}}$ at the outer boundary.
The method of choice for solving such an equation was shooting based upon a fourth order Runge-Kutta method and it since has become the test-bed calculation against which other methods (to be used for the full two-dimensional calculation) are compared.

If one finite differences the lapse equation with a standard second order differencing for the first and second derivatives with respect to η, the result is a linear system of algebraic equations which can be written in matrix notation as $\mathbf{M}\alpha=\mathbf{b}$. Here the square matrix **M** is a tridiagonal matrix that contains the coefficients resulting from the finite differencing of the lapse equation, α is a vector whose components are the values of the lapse at the grid points, and **b** is also a vector of the same length that contains the values of

the lapse at the boundaries. Methods used to solve the matrix equation and tested against the shooting method have been 1.) simultaneous over relaxation (SOR), 2.) direct Gaussian elimination with pivoting and interchange of rows 3.) an iterative conjugate gradient method with different preconditionings. All of the matrix methods except SOR (which eventually took so long to converge it could not make the required cut off of 20000 time steps) gave the same results as the shooting method (to within one tenth of one percent or less) on radial grids with 1000 and 2000 nodes.

The differencing of the hyperbolic equations produced significantly different results depending upon the schemes employed. Rather than write out the full finite differenced versions of the Einstein equations appearing in the Appendix, we shall write the evolution equations in the schematic form: $\partial_t g = -2\alpha K$ and $\partial_t K = \alpha(K^2+R) + \Delta\alpha$. N.B. the symbols K and R are *not* the contracted extrinsic and intrinsic curvatures, $\Delta\alpha$ will represent the covariant Hessian of the lapse and for the sake of simplicity, we have eliminated the terms involving the shift since they may be treated in the same manner as the lapse. The grid is unstaggered in space but depending upon the finite difference scheme, may be staggered in time.

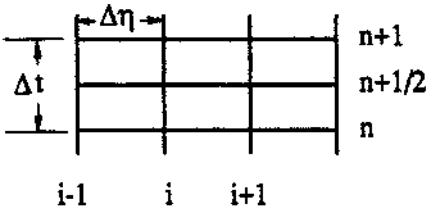


Figure 1. The numerical grid used for the finite differencing methods discussed in the text.

In all, nine different methods for finite differencing the evolution equations were utilized. The first order schemes used were a standard forward-time, centered-space method (FTCS) and the Lax method. The FTCS scheme is

$$g_i^{n+1} = g_i^n - 2\alpha_i^n K_i^n \Delta t \quad \text{and} \quad K_i^{n+1} = K_i^n + \{\alpha_i^n [(K_i^n)^2 + R_i^n] - (\Delta\alpha)_i^n\}\Delta t$$

and the Lax method, by averaging the variables on the nth time step, introduces an implicit artificial viscosity:

$$g_i^{n+1} = \tfrac{1}{2}(g_{i-1}^n + g_{i+1}^n) - 2\alpha_i^n K_i^n \Delta t\,; \quad K_i^{n+1} = \tfrac{1}{2}(K_{i-1}^n + K_{i+1}^n) + \{\alpha_i^n[(K_i^n)^2 + R_i^n] - (\Delta\alpha)_i^n\}\Delta t$$

In both of these cases, the first and second spatial derivatives of the metric that appear in the Ricci tensor and the Hessian of the lapse, $\Delta\alpha$ are all central differenced about the point, i, on the time step, n; i.e. $\partial_\eta g = (g_{i+1}^n - g_{i-1}^n)/(2\Delta\eta)$ and $\partial_{\eta\eta} g = (g_{i+1}^n - 2g_i^n + g_{i-1}^n)/(\Delta\eta)^2$.

Variations on the leapfrog scheme were implemented as well. The metric evolution was straight forward, but different methods were used to treat the nonlinear term in K for the extrinsic curvature evolution equation. The first method simply used the value of K on the previous time step and this added first order errors to the method:

$$g_i^{n+1/2} = g_i^{n-1/2} - 2\alpha_i^n K_i^n \Delta t \quad \text{and} \quad K_i^{n+1} = K_i^n + \{\alpha_i^n [(K_i^n)^2 + R_i^{n+1/2}] - (\Delta\alpha)_i^n\}\Delta t$$

In order to improve upon the method and make it completely second order in both temporal and spatial derivatives, the terms in the K evolution equation that are determined on the nth time step by the evolution equations need to be evaluated on the time step, n+1/2. This change makes the scheme a fully staggered leapfrog without introducing first order errors. To accomplish this one replaces the evolution equation for the extrinsic curvature with:

$$K_i^{n+1} = K_i^n + \{{}^*\alpha_i^n[({}^*K_i^{n+1/2})^2 + R_i^{n+1/2}] - ({}^*\Delta\alpha)_i^{n+1/2}\}\Delta t$$

where the starred quantities were calculated from a $\Delta t/2$ step extrapolation defined by ${}^*u_i^{n+1/2} = \frac{3}{2}u_i^n - \frac{1}{2}u_i^{n-1}$.

Three two-step methods were used and these eventually led to true predictor-corrector schemes. While these schemes have the disadvantage of requiring more storage, they are provide better stability and can be run longer. Perhaps the best known of the two-step methods is the Lax-Wendroff scheme which consists of a Lax method for a one-half time step and then a leapfrog for a full time step:

(1) $g_i^{n+1/2} = \frac{1}{2}(g_{i-1}^n + g_{i+1}^n) - 2\alpha_i^n K_i^n\,(\Delta t/2)$;

$K_i^{n+1/2} = \frac{1}{2}(K_{i-1}^n + K_{i+1}^n) + \{\alpha_i^n[(K_i^n)^2 + R_i^n] - (\Delta\alpha)_i^n\}\,(\Delta t/2)$

(2) $g_i^{n+1} = g_i^n - 2{}^*\alpha_i^{n+1/2} K_i^{n+1/2}\Delta t$

$K_i^{n+1} = K_i^n + \{{}^*\alpha_i^{n+1/2}[(K_i^{n+1/2})^2 + R_i^{n+1/2}] - ({}^*\Delta\alpha)_i^{n+1/2}\}\Delta t$

In this scheme the extrapolation of the values for K is unnecessary since they are determined by the Lax method. The value of the lapse on the (n+1/2)th time step is still determined by half-step extrapolation. Two variations on this scheme are 1.) replace the Lax method with a FTCS scheme and 2.) implement a full time step "double" leapfrog which can be considered as a simple predictor-corrector scheme. This latter two step method can be written in the form:

(1) $g_i^{n+1/2} = g_i^{n-1/2} - 2\alpha_i^n K_i^n\,\Delta t$

$K_i^{n+1/2} = K_i^{n-1/2} + \{\alpha_i^n[(K_i^n)^2 + R_i^n] - (\Delta\alpha)_i^n\}\,\Delta t$

(2) $g_i^{n+1} = g_i^n - 2\alpha_i^{n+1/2} K_i^{n+1/2}\Delta t$

$K_i^{n+1} = K_i^n + \{\alpha_i^{n+1/2}[(K_i^{n+1/2})^2 + R_i^{n+1/2}] - (\Delta\alpha)_i^{n+1/2}\}\Delta t$

After performing the first leapfrog calculation, the maximal slicing equation is solved on the n+1/2 time step and the result is used in the next leapfrog calculation to obtain the value of R for a subsequent calculation of the lapse. This method has the disadvantage of having to solve the lapse equation twice at each time level.

Finally two fully-second order predictor-corrector methods were employed. These two methods are now commonly employed in hydrodynamics codes, but as far as we know they have not been used extensively in numerical relativity, if at all. The better known of the two is the method of MacCormack:

(1) $\tilde{g}_i^{n+1} = g_i^n - 2\alpha_i^n K_i^n\,\Delta t$ predictor

$\tilde{K}_i^{n+1} = K_i^n + \{\alpha_i^n[(K_i^n)^2 + R_i^n] - (\Delta\alpha)_i^n\}\,\Delta t$

(2) $g_i^{n+1} = \frac{1}{2}[\,\tilde{g}_i^{n+1} + g_i^n - 2\alpha_i^n \tilde{K}_i^{n+1}\,\Delta t\,]$ corrector

$K_i^{n+1} = \frac{1}{2}[\,\tilde{K}_i^{n+1} + K_i^n + \{\alpha_i^n[(\tilde{K}_i^{n+1})^2 + \tilde{R}_i^{n+1}] - (\tilde{\Delta}\alpha)_i^{n+1}\}\Delta t]$

The MacCormack method differs from all other schemes that have been described up to now. It is distinguished by the fact that in the predictor equations, the first spatial derivatives of the metric appearing in the Ricci tensor and Hessian of the lapse are determined by forward differencing: $\partial_\eta g = (g_{i+1}^n - g_i^n)/\Delta\eta$. In the corrector equations these derivatives are calculated using backwards differencing: $\partial_\eta g = (g_i^n - g_{i-1}^n)/\Delta\eta$. An alternative

method is to backward difference at the predictor level and forward difference the corrector equation. Second derivatives are always centered differenced.

On the other hand, the method of Brailovskaya, uses a centered differencing scheme for spatial derivatives in both the predictor and corrector equations.

(1) $\tilde{g}_i^{n+1} = g_i^n - 2\alpha_i^n K_i^n \Delta t$ predictor

$\tilde{K}_i^{n+1} = K_i^n + \{\alpha_i^n[(K_i^n)^2 + R_i^n] - (\Delta\alpha)_i^n\} \Delta t$

(2) $g_i^{n+1} = g_i^n - 2\alpha_i^n \tilde{K}_i^{n+1} \Delta t$ corrector

$K_i^{n+1} = K_i^n + \{\alpha_i^n[(\tilde{K}_i^{n+1})^2 + \tilde{R}_i^{n+1}] - (\tilde{\Delta}\alpha)_i^{n+1}\} \Delta t$

and is somewhat easier to code.

IV. ANALYTIC BEHAVIOR OF THE SCHWARZSCHILD SOLUTION APPROPRIATE TO NUMERICAL RELATIVITY

As every student of general relativity knows, the Schwarzschild solution is static. However if one slices the 4-dimensional spherical black hole space time by time slices that do not preserve the isometry of the 3-spatial geometry from one time slice to the next, the spacetime will appear to be time dependent since the spatial geometry changes from slice to slice. This is precisely what can happen in numerical relativity. A good illustration of how the spacelike surfaces depend upon the choice of constant time slices is found in Chapter 31 (p 839) of Misner, Thorne and Wheeler (1973), where different slices across the Kruskal diagram for the Einstein-Rosen bridge produce strikingly different results.

The initial data is for a single black hole is simple and its extension to multiple black holes is discussed by York in this volume. Using the York prescription for solving the initial value problem, imposing time-symmetry ($K_{ij}=\beta=0$) and conformal flatness (a=b=1 which implies the vanishing of the scalar curvature), one need only solve the flat space Laplacian for ψ' to obtain $\psi' = (1+\frac{m}{2r'})$. This solution describes the static Einstein-Rosen bridge. While this can be represented in a number of different coordinate systems (Kruskal-Szekeres, Novikov, and Eddington-Finkelstein to name but a few), we shall use the isotropic coordinates given in eq. (2.3). At the throat r'=m/2 (r=2m), one can identify the $m/2>r'>0$ with $m/2<r^*<\infty$ with the relationship $r^* = m^2/(4r')$ which gives the static two sheeted version of the Schwarzschild solution where the interior is mapped onto an asymptotically flat spacetime.

The slices that represent the static time translations should be reproduced easily since there is no evolution. In terms of the numerical metric the isotropic gauge can be written in the following form:

$$\alpha = \tanh(\eta/2) \qquad \psi = 2\sqrt{m/2}\cosh(\eta/2) \qquad a=b=1 \qquad (4.1)$$

These results are used as an initial test (albeit a rudimentary one) of the code. As such it tests mainly for simple errors (typographical, missing terms, etc.) since the lapse in eq. (4.1) must keep the metric and extrinsic curvature from evolving from one slice to the next. This will only result if the Ricci tensor (depending only upon derivatives of the conformal factor) exactly cancels the Hessian of the lapse.

Another well-known behavior associated with the Schwarzschild solution is that one can analytically calculate the radial geodesics and the motion of a test particle falling along them. If the test particle is at a position $R=r_0/2m$ where r_0 is the usual Schwarzschild coordinate, at time $t=0$ (proper time $\tau=0$) then the resulting position in Schwarzschild coordinates (r,t) after proper time,τ, has elapsed is given in the parametric form (see e.g. MTW):

$$\tau = mR^{3/2}(\lambda + \sin\lambda), \qquad r = mR(1+\cos\lambda)$$

$$t/2m = \ln\left(\frac{\sqrt{R-1}+\tan(\lambda/2)}{\sqrt{R-1}-\tan(\lambda/2)}\right) + \sqrt{R-1}\left[\lambda + \tfrac{1}{2}R(\lambda+\sin\lambda)\right] \qquad (4.2)$$

Clearly the after an elapsed proper time $\tau=\pi mR^{3/2}$, the test particle has fallen into the central singularity ($\lambda=\pi$). This result can prove to be an important check on the numerical results of a code. If one sets the gauge to geodesic normal slicing ($\alpha=1$, $\beta=0$), the grid points free fall radially into the black hole. The initial data surface at the moment of time symmetry is described by the normal Einstein-Rosen bridge configuration where the throat is located at the Schwarzschild radius, $r=2m$. According to eqs. (4.2) this grid point will fall into the central singularity after an elapsed time of πm, at which time the code crashes. Making a crash test of the code during the initial stages of development, like the crash testing of automobiles, yields important information before a prototype is turned into a finished product. Oddly enough some codes failed even at this early a stage in development. The first order methods and the leapfrog without time step extrapolation did not crash until a few time steps after $\tau=\pi m$.

Finally, the most important analytic results concern the behavior of the maximally sliced ($TrK=0$) Schwarzschild solution. The static isotropic coordinates in eq. (2.3) are an example of a maximally sliced Schwarzschild solution. The lapse function is a solution of eq. (2.6) (K_{ij} vanishes due to the time symmetry and R_{ij} is determined solely from the conformal factor) given the Dirichlet boundary conditions $\alpha=0$ at the throat. If on the other hand the boundary conditions are Neumann conditions, with $\partial_\eta\alpha=0$ at the throat, the lapse is time dependent and must collapse to zero in order to prevent the grid from falling into the Schwarzschild singularity. The time dependent behavior of the lapse function at the throat was calculated by Smarr and York (1978) using a simplified model and was found to be $\alpha_{min}=\exp(-\tau/\tau_e)$ where the e-folding time $\tau_e \cong 1.82m$. It has been argued by some that since the lapse collapses rapidly in the interior of the black hole, the physics is occurring at such a slow rate, that one may be able to simply replace the values of the lapse at the throat and its neighboring grid points with zero after some predetermined time in the evolution. However, had we performed such a procedure right from the start we would not have been able to determine the appropriate differencing schemes and minimum step size needed to reproduce the analytic behavior.

Another important result was reached in the work of Estabrook, et. al. (1974), who proved that for the dynamic maximal slicing of the Schwarzschild solution, the grid points asymptotically fall to the surface defined by the Schwarzschild radius, $r=\frac{3}{2}m$ which is itself maximal. This behavior can be understood qualitatively as follows: The initial hypersurface has the metric of a 3-parabaloid. (If it were a 2-parabaloid it would have

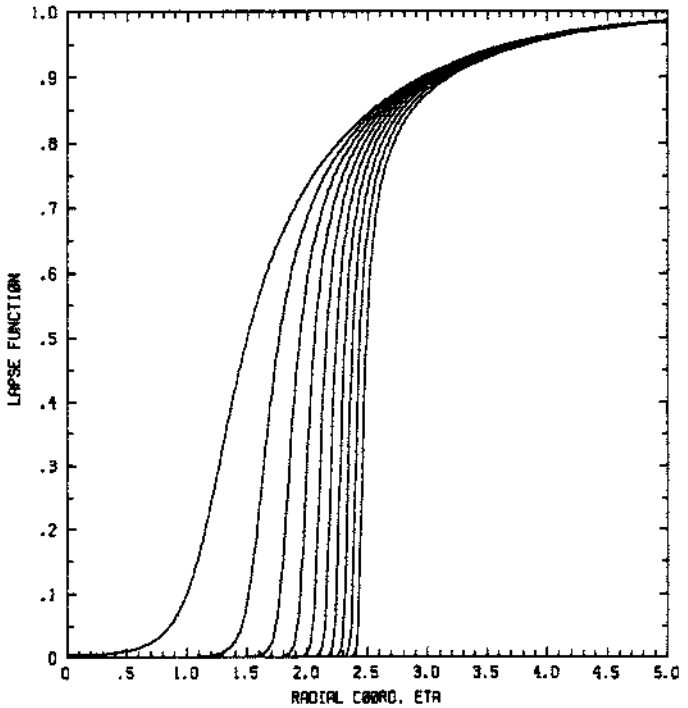


Figure 2. The lapse function for a dynamical maximally sliced Schwarzschild spacetime at time intervals of 10m from t=0 to t=100m. Most of the collapse of the lapse occurs within the first 10m of the evolution. Problems with maximal slicing occur when the spatial derivatives of the lapse grow at late times.

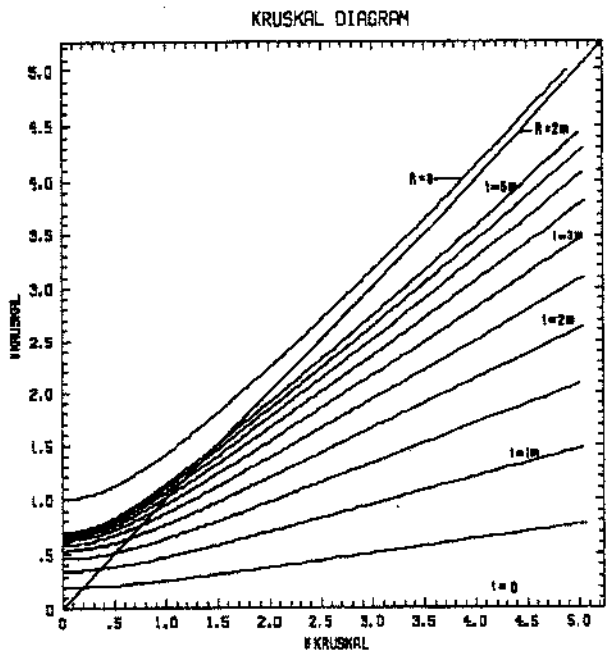


Figure 3. A Kruskal diagram showing the t=const maximal slices for the Schwarzschild spacetime. The slices at late times pile up at r=3m/2 in the inner region but still have to reach outside of the horizon at r=2m. This causes the grid stretching problems associated with maximal slicing. The slices are shown at time intervals of .5m from t=0 to t=5m. After 5m the inner region does not evolve significantly.

negative scalar curvature). As soon as the hypersurface begins to evolve, the bridge begins to stretch and and its central portion assumes the shape of a 3-cylinder (which has positive scalar curvature: essentially that of its generating 2-spheres). Since R is now positive, the lapse becomes concave upwards with increasing η in the region near the throat (see eq. (2.6)). Therefore it starts to collapse to zero, which eventually stabilizes the bridge in the throat region. The 3-scalar curvature of a cylindrical surface is $R=2/r^2$. Therefore at r=3m/2 one has $R=\frac{8}{9m^2}$. One may also use the results of eqs. (3.2) for the behavior of the freely falling test particles to calculate the total proper time for the throat to collapse from r=2m to the r=3m/2 ($\lambda=\pi/3$) and obtain $\tau_{max}=\int_0^\infty \alpha_{min}\, d\tau = (\frac{\pi}{3}+\frac{\sqrt{3}}{2})m \cong 1.9132m$. It must be remembered that those points which are initially outside of the black hole event horizon have time-like trajectories that are affected by the effective acceleration produced by the lapse and therefore will not obey eqs. (3.2).

Figures 2 and 3 typify the behavior of the maximally sliced spherically symmetric solution. The collapse of the lapse for each 10m in time from t=10m to t=100m are shown in Figure 2. The outer boundary was placed at $\eta=10$ (or a Schwarzschild radius of about 11000m) and the step sizes were Δt =.005m and $\Delta\eta=0.01$. In order to avoid the singularity, the value of the lapse at the throat collapses to 10^{-2} by 5m in coordinate time. Initially the lapse is set to unity for all values of η. The behavior of the spatial slices can be represented by a Kruskal diagram (Figure 3) where the maximal t=const slices clearly halt at r=3m/2 and wrap themselves about the central r=0 singularity. The time slices in Figure 3 are shown at intervals of .5m from t=0 to t=5m.

The analytic results of Smarr and York (1978) for the 'collapse of the lapse' can be checked by plotting the logarithm of the lapse function at the throat versus time and determining the e-folding time. This measurement is also dependent upon the size of the time step as well. Figures 4a and 4b show the results for some of the finite difference methods described in the previous section. Calculations were performed that used time steps of .01m and .005m. Clearly the numerical dispersion that results from larger step sizes will ruin the accuracy of the computation at late times. The effect is particularly apparent for the Lax and Lax-Wendroff methods which introduce an implicit artificial viscosity into the code. The second order methods themselves are subject to dispersion and after 40000 time steps (t=200m for Δt =.005m) the strictly exponential behavior begins to die off with $\alpha \approx 10^{-94}$. Finally the e-folding time calculated for the second-order methods from Figure 4b yields τ_e=1.821 compared to the Smarr-York value of 1.82.

Checking the results concerning the singularity avoidance of maximal slicing we calculate the total proper time elapsed at the throat during the evolution from t=0 to t=100m (with a time step of .005m) using a Simpson's rule integration procedure. We also determined the value of the Schwarzschild radius at the throat (for t=100m) and compare that to the analytic value of 1.5m. Since the limiting hypersurface at late times is a 3-cylinder we must also verify that the points at $\eta>0$ lie close to that cylinder with radius 3m/2. The numerical evolution proceeds only to a finite value of time. Therefore one would expect that the 3-surfaces have not yet reached the asymptotic cylindrical topology.

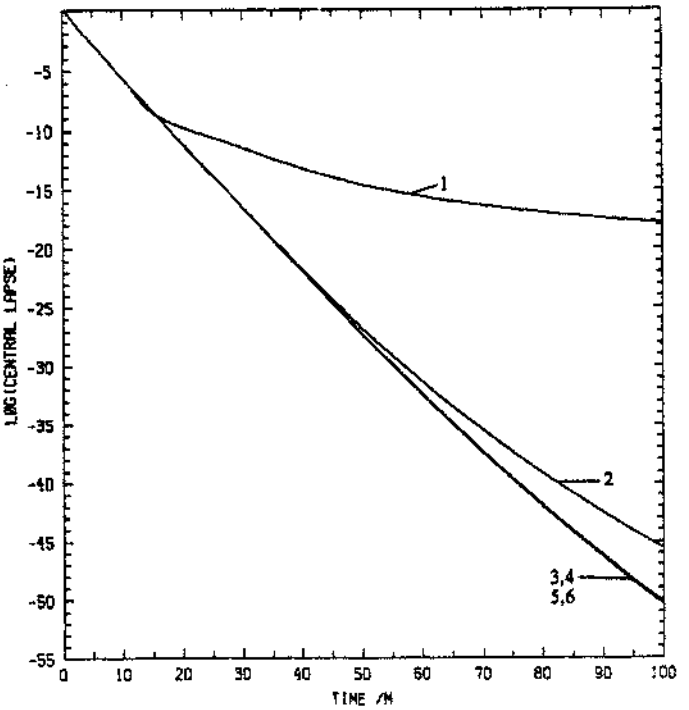


Figure 4a. The time dependent behavior of the lapse function at the throat calculated with different finite difference methods with Δt=.01m. The methods used are 1. Lax; 2. Lax-Wendroff; 3. Leapfrog with 1/2 time step extrapolation; 4. two step FTCS-Leapfrog; 5. MacCormack; 6. Brailovskaya.

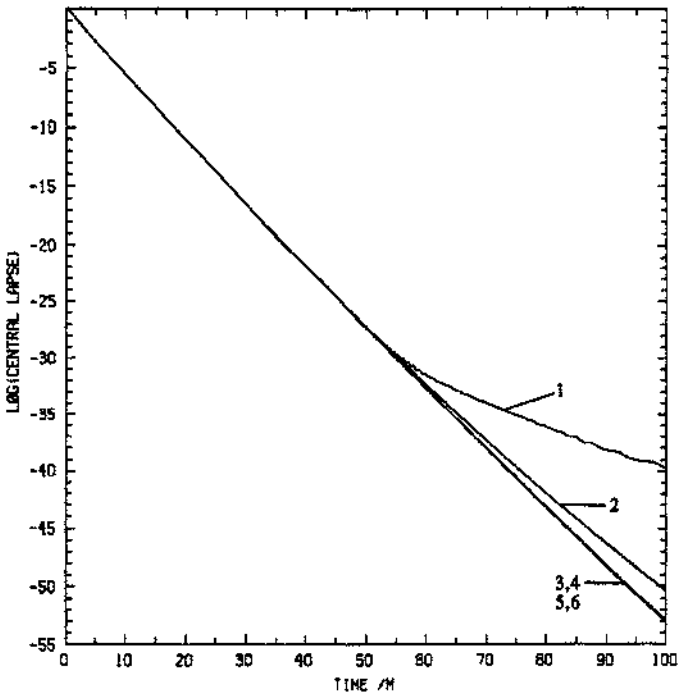


Figure 4b. The same graph as in Figure 4a but with Δt=.005m. Better agreement with the analytic results are obtained with the finer resolution. The e-folding time is determined to be τ_e=1.821m.

Those grid points that at t=0 were originally outside of the event horizon ($\eta>0$) should at late (but finite) times be located at Schwarzschild radii somewhat greater than 3m/2. If there is no crossing of the grid points then the value of the Schwarzschild radius will monotonically increase with the coordinate η. For many of the finite differencing schemes this did not occur. Some points located at $\eta>0$ were found to have a of the Schwarzschild radius less than the value of the Schwarzschild radius at the throat ($\eta=0$) for t > 50m in the evolution. The results of the test of proper time and monotonicity of the Schwarzschild radius for different finite differencing schemes are presented in Table 1.

finite differencing scheme	total proper time elapsed @ throat	R Schwarz. $\eta=0$ (t=100m)	R Schwarz. monotone @ $\eta>0$
Analytic	**1.9132m**	**1.50000m**	**yes**
Lax	1.9261m	1.48992m	no
FTCS	1.9223m	1.49548m	no
Leapfrog (1st ord. error)	1.9204m	1.49835m	no
Leapfrog (1/2 step extrap.)	1.9132m	1.49999m	no
Two time step Leapfrog	1.9132m	1.49998m	no
FTCS-Leapfrog	1.9174m	1.49968m	no
Lax-Wendroff	1.9212m	1.49727m	yes
McCormack	1.9132m	1.49999m	yes
Brailovskaya	1.9132m	1.49999m	yes

Table1. The results of the collapse of throat and points just outside of the horizon during the evolution to t=100m for the maximally sliced Schwarzschild solution. The step sizes were chosen as Δt=.005m and $\Delta\eta$=.01. The outer boundary was placed at η=10.

The results of Table 1 and Figure 4b can be summarized as follows. For those differencing methods that are more dispersive, the lapse does not collapse as rapidly as it should thereby allowing the evolution to proceed longer than expected in the region of the throat. This results in both a longer elapsed proper time and a limiting Schwarzschild radius of less than 3m/2. While four of the second order methods agree quite closely with the analytic results, it is only the two predictor-corrector methods that passed all tests. It should be noted that at t=100m, the limiting value of the Schwarzschild radius is less than 3m/2 for all methods. Part of the reason for this is that no method is completely free of dispersive effects and even at t=100m there is some deviation from exponential drop off of the lapse at the throat.

Our present philosophy is that if a numerical relativity code is expected to accurately reproduce known analytic results, then one result that the code should also be expected to reproduce is the propagation of the constraints by the evolution equations. If free evolution is properly carried out then the constraints should act as a check on how accurately one is solving the entire Einstein system. Analytically we know that the Einstein equations form a self consistent system and that self consistency should be maintained in the finite differenced version as well. For the believers in constrained evolution, where the constraint equations are used to determine some of the dependent variables, the self consistency check involves a verification that the extra evolution equations are satisfied.

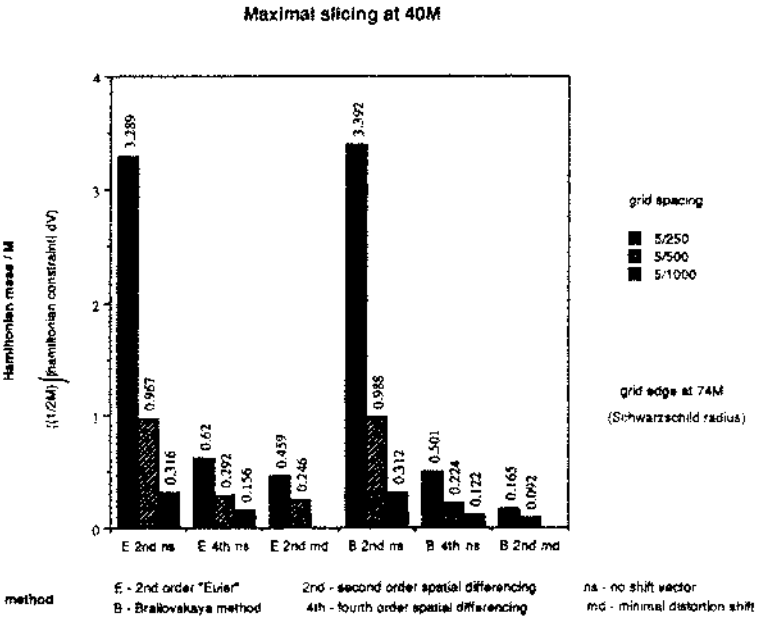


Figure 5. The Hamiltonian constraint integrated over the entire computational spacelike hypersurface. This provides a measure of how large the errors are in propagating the constraints with a free evolution. The minimal distortion shift vector combined with a higher order predictor-corrector method is necessary to maintain the constraints.

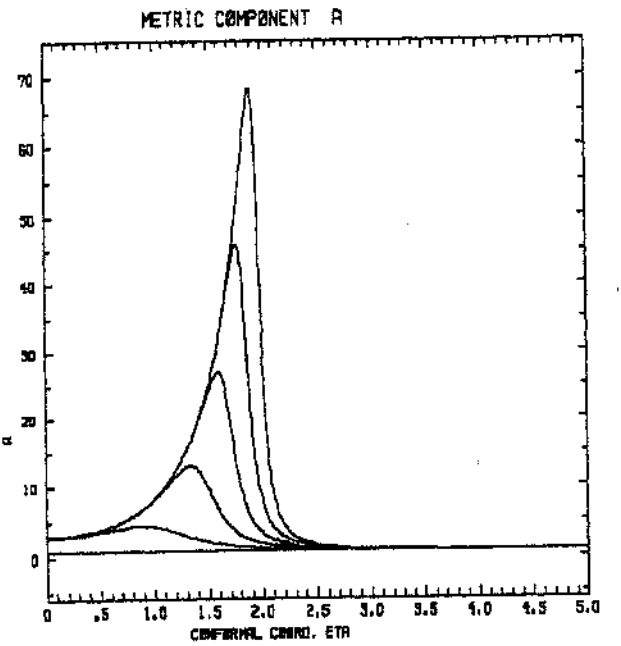


Figure 6. The radial metric coefficient from t=0 to t=40m with maximal slicing and vanishing shift vector. The coordinate shear at late times causes the metric to grow without bound in the vicinity of the event horizon. This eventually causes that code to halt at times greater than t=200m.

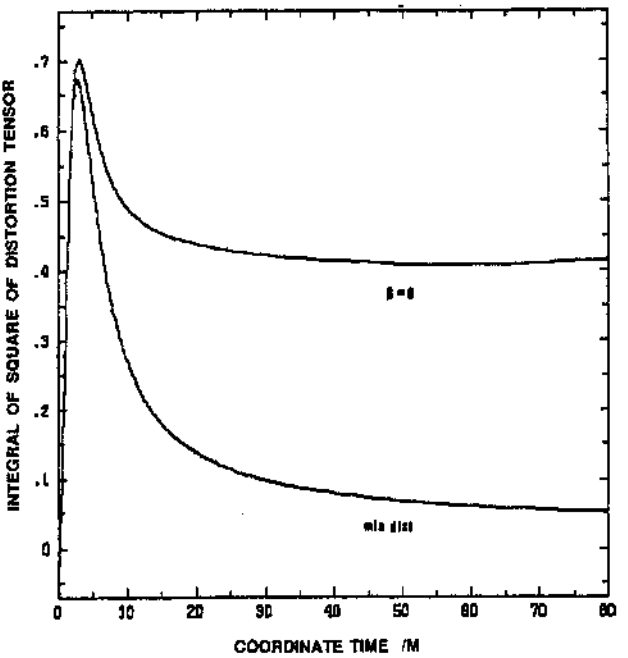


Figure 7. The integrated value of the square of the distortion tensor as a function of coordinate time. This demonstrates that the minimal distortion shift vector does reduce much of the coordinate shear.

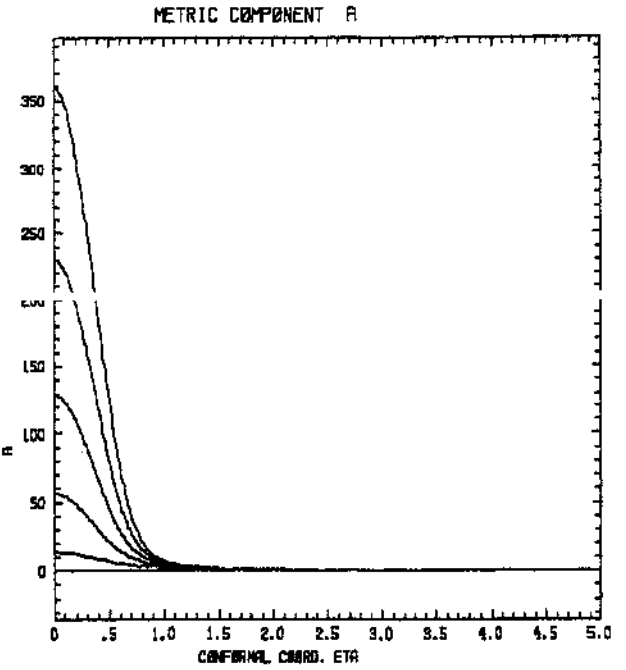


Figure 8. The radial metric coefficient from t=0 to t=40m with maximal slicing and minimal distortion shift vector. The coordinate shear at late times is shifted to the throat and the growth of the radial metric at this location occurs so rapidly that the evolution is halted soon after t=40m.

Since our intended purpose is to develop better methods of handling the hyperbolic equations, we have chosen to use the constraints as a check on free evolution. Figure 5 shows the results of a selected number of tests where the integrated value of the hamiltonian constraint is compared to the total mass of the system. While the absolute values of the constraints may actually be small, the integrated value over the hypersurface will give a better measure of how much 'energy' is associated with inaccuracies in numerical methods.

The important results of Figure 5 are that fourth order spatial differences are better at propagating the constraints than the simple second order difference methods. The reason why the spatial differencing is so important is that as the lapse collapses during the late time evolution, its spatial derivatives along with the spatial derivatives of the 3-metric and extrinsic curvature need to be calculated with ever increasing accuracy. The gradients of all the metric and extrinsic curvature components become very large in the vicinity of the event horizon if the shift vector vanishes (see Figure 2). Unless one has accurate methods of taking derivatives in the vicinity of these steep gradients, the code will quickly fail. The improved accuracy of the predictor-corrector methods clearly win out in this case.

While the leapfrog method has become the workhorse for finite differencing schemes in numerical relativity, its disadvantages outweigh its advantages when compared to the Brailovskaya or MacCormack predictor-corrector methods. The extra amount of effort that is needed to encode these latter two-step methods is negligible compared to the accuracy and stability that they provide.

At very late times ($t > 200m$) even the most accurate maximal slicing methods failed. As can be seen in Figure 6, the radial metric component develops a sharp peak in the vicinity of the event horizon and the finite difference approximation of the steep gradients eventually breaks down, forcing the code to halt. Smarr and York (1978) proposed the minimal distortion shift condition in order to overcome these problems. While the minimal distortion shift vector does reduce a measure of the distortion the (see Figure 7 which plots the square of the distortion tensor integrated over the 3-surface as a function of time) and removes the sharp gradients of the radial metric component in the region of the event horizon, the coordinate shear is transferred to the throat (where the volume elements are small) and produces even larger gradients. This behavior is shown in Figure 8 and is to be compared to figure 6. As a result, the minimal distortion shift condition caused the code to terminate at about 80m.

It is clear that numerically simulating black hole spacetimes with dynamic, singularity avoiding spacelike slices is not a trivial problem and more work remains to be done if longer and more accurate time evolutions are to be performed. Part of the problem may be blamed upon the use of a logarithmic radial variable. While it conveniently covers the region far outside the black hole it inadequately covers the region near the horizon. A partial cure may be found in the use of adaptive grids that allow the horizon (or any other region where large gradients form) to be covered with a greater degree of accuracy.

Our efforts have come closer to obtaining the Holy Grail of numerical relativity (Shapiro and Teukolsky (1986)). By definition the black hole codes we have written avoid singularities and treat black holes. With some combination of minimal principles, adaptive gridding, and perhaps higher order predictor-corrector methods, higher accuracy and longer term stability may finally be achieved.

V. FUTURE WORK

A two dimensional code that will be used to calculate the head-on collision of two black holes has been written using the methods described in this article. Deriving and coding a two-dimensional code based upon the most general three-metric possible is a project that can certainly introduce many errors. However using Macsyma we were able to derive the equations and translate many of the expressions into optimized Cray Fortran code. This meant altering the source code for the Macsyma tensor packages somewhat but since they are written in the Macsyma language, this proved to be a simpler job than had originally been expected.

The first test of the two-dimensional code, outside of reproducing all of the results presented here, will be to reproduce the normal mode analysis of an oscillating black hole. Analytic initial data exists for a single black hole superimposed on any number of gravitational multipole moments. While some of the contributions to the initial distortion of the gravitational field can be considered to result from incoming gravitational radiation, it is likely that most of this will leave the system quickly [see Schutz (1980) and Anderson and Hobill (1988) for arguments] and leave behind an oscillating black hole that loses its distortion through quasi-normal mode 'ringing'. It is hoped that the accuracy and stability of the code will be such that the numerical solution will be able to pick out the gravitational wave tails that exist long after the first burst of radiation is emitted.

If the amplitudes of the initial multipole moments are large enough, the pertubative results should break down. One goal is to determine when this occurs. A single oscillating black hole is expected form after two colliding black holes have merged. Therefore the next stage on the way to the development of a two black hole collision code will also provide an important test-bed calculation to guide the development of future codes designed to study black hole spacetimes.

REFERENCES

Anderson, J.L., and Hobill, D. W., (1988), *J. Comp. Phys.*, **75**, 283.
Bardeen, J., and Piran, T., (1983), *Phys. Reports.*, **96**, 205.
Cadez, A., (1971) Ph. D. Thesis, University of North Carolina
Choptuik, M., (1986), Ph. D. Thesis, University of British Columbia.
Eardley D., and Smarr, L., (1979) *Phys. Rev. D.*, **19**, 127.
Estabrook, F., Wahlquist, H., Christensen, S., DeWitt, B., Smarr, L., and Tsiang, E., (1973), *Phys. Rev. D.*, **7**, 2814.
Evans, C., (1986), In *Dynamical Spacetimes and Numerical Relativity*, edited by Centrella, J., Cambridge University Press, Cambridge.
Hahn, S. G. and Lindquist, R. W., (1964), *Ann. Phys.*, **29**, 304.
Misner, C.W., Thorne, K.S., and Wheeler, J. A., (1973), *Gravitation*, W. H. Freeman, San Francisco.
Shapiro, S. and Teukolsky, S., (1986), In *Dynamical Spacetimes and Numerical Relativity*, edited by Centrella, J., Cambridge University Press, Cambridge.
Schutz, B., (1980), *Phys. Rev. D.*, **22**, 249.
Smarr, L., (1979), In *Sources of Gravitational Radiation*, edited by Smarr, L., Cambridge University Press, Cambridge.
Smarr, L., and York, J., (1978), *Phys. Rev. D.*, **17**, 2529.
Wilson, J., (1979), In *Sources of Gravitational Radiation*, edited by Smarr, L., Cambridge University Press, Cambridge.

APPENDIX: VACUUM EINSTEIN EQUATIONS FOR SPHERICAL SYMMETRY

$$R_{\eta\eta}=-\frac{4\frac{\partial^2\psi}{\partial\eta^2}}{\psi}+\frac{4\left[\frac{\partial\psi}{\partial\eta}\right]^2}{\psi^2}-\frac{2\frac{\partial b}{\partial\eta}\frac{\partial\psi}{\partial\eta}}{b\psi}+\frac{2\frac{\partial a}{\partial\eta}\frac{\partial\psi}{\partial\eta}}{a\psi}-\frac{\frac{\partial^2 b}{\partial\eta^2}}{b}+\frac{\left[\frac{\partial b}{\partial\eta}\right]^2}{2b^2}+\frac{\frac{\partial a}{\partial\eta}\frac{\partial b}{\partial\eta}}{2ab}$$

$$R_{\xi\xi}=-\frac{2b\frac{\partial^2\psi}{\partial\eta^2}}{a\psi}-\frac{2b\left[\frac{\partial\psi}{\partial\eta}\right]^2}{a\psi^2}-\frac{3\frac{\partial b}{\partial\eta}\frac{\partial\psi}{\partial\eta}}{a\psi}+\frac{\frac{\partial a}{\partial\eta}b\frac{\partial\psi}{\partial\eta}}{a^2\psi}-\frac{\frac{\partial^2 b}{\partial\eta^2}}{2a}+\frac{\frac{\partial a}{\partial\eta}\frac{\partial b}{\partial\eta}}{4a^2}+1$$

Hamiltonian constraint

$$0=\frac{2R_{\xi\xi}}{b\psi^4}+\frac{R_{\eta\eta}}{a\psi^4}+\frac{2H_b^2}{b^2}+\frac{4H_aH_b}{ab}$$

momentum constraint

$$0=\frac{4H_b\frac{\partial\psi}{\partial\eta}}{b\psi}-\frac{4H_a\frac{\partial\psi}{\partial\eta}}{a\psi}+\frac{2\frac{\partial H_b}{\partial\eta}}{b}-\frac{\frac{\partial b}{\partial\eta}H_b}{b^2}-\frac{\frac{\partial b}{\partial\eta}H_a}{ab}$$

evolution equations

$$\frac{\partial a}{\partial t}=\frac{4\beta\frac{\partial\psi}{\partial\eta}}{\psi^5}+\frac{2\frac{\partial\beta}{\partial\eta}}{\psi^4}-\frac{\frac{\partial a}{\partial\eta}\beta}{a\psi^4}-2\alpha H_a$$

$$\frac{\partial b}{\partial t}=\frac{4b\beta\frac{\partial\psi}{\partial\eta}}{a\psi^5}+\frac{\frac{\partial b}{\partial\eta}\beta}{a\psi^4}-2\alpha H_b$$

$$\frac{\partial H_a}{\partial t}=\frac{\alpha R_{\eta\eta}}{\psi^4}-\frac{4\beta H_a\frac{\partial\psi}{\partial\eta}}{a\psi^5}+\frac{2\frac{\partial\alpha}{\partial\eta}\frac{\partial\psi}{\partial\eta}}{\psi^5}+\frac{\beta\frac{\partial H_a}{\partial\eta}}{a\psi^4}+\frac{2\frac{\partial\beta}{\partial\eta}H_a}{a\psi^4}-\frac{2\frac{\partial a}{\partial\eta}\beta H_a}{a^2\psi^4}-\frac{\frac{\partial^2\alpha}{\partial\eta^2}}{\psi^4}+\frac{\frac{\partial a}{\partial\eta}\frac{\partial\alpha}{\partial\eta}}{2a\psi^4}+\frac{2\alpha H_aH_b}{b}-\frac{\alpha H_a^2}{a}$$

$$\frac{\partial H_b}{\partial t}=\frac{\alpha R_{\xi\xi}}{\psi^4}+\frac{4\beta H_b\frac{\partial\psi}{\partial\eta}}{a\psi^5}-\frac{2\frac{\partial\alpha}{\partial\eta}b\frac{\partial\psi}{\partial\eta}}{a\psi^5}+\frac{\beta\frac{\partial H_b}{\partial\eta}}{a\psi^4}-\frac{\frac{\partial\alpha}{\partial\eta}\frac{\partial b}{\partial\eta}}{2a\psi^4}+\frac{\alpha H_aH_b}{a}$$